2632–2643 *Nucleic Acids Research, 2013, Vol. 41, No. 4* *Published online 8 January 2013*
doi:10.1093/nar/gks1315

Competitive folding of anti-terminator/terminator hairpins monitored by single molecule FRET

Caroline Clerte, Nathalie Declerck and Emmanuel Margeat*

CNRS UMR5048, Centre de Biochimie Structurale, 29 rue de Navacelles, 34090 Montpellier, France; INSERM U1054, 34090 Montpellier, France; and Universités Montpellier I et II, 34090 Montpellier, France

Received October 22, 2012; Revised November 15, 2012; Accepted November 16, 2012

ABSTRACT

The control of transcription termination by RNA-binding proteins that modulate RNA-structures is an important regulatory mechanism in bacteria. LicT and SacY from *Bacillus subtilis* prevent the premature arrest of transcription by binding to an anti-terminator RNA hairpin that overlaps an intrinsic terminator located in the 5′-mRNA leader region of the gene to be regulated. In order to investigate the molecular determinants of this anti-termination/termination balance, we have developed a fluorescence-based nucleic acids system that mimics the competition between the LicT or SacY anti-terminator targets and the overlapping terminators. Using Förster Resonance Energy Transfer on single diffusing RNA hairpins, we could monitor directly their opening or closing state, and thus investigate the effects on this equilibrium of the binding of anti-termination proteins or terminator-mimicking oligonucleotides. We show that the anti-terminator hairpins adopt spontaneously a closed structure and that their structural dynamics is mainly governed by the length of their basal stem. The induced stability of the anti-terminator hairpins determines both the affinity and specificity of the anti-termination protein binding. Finally, we show that stabilization of the anti-terminator hairpin, by an extended basal stem or anti-termination protein binding can efficiently counteract the competing effect of the terminator-mimic.

INTRODUCTION

Transcription termination that marks the end of transcription by the RNA polymerase (RNAP) and transcription anti-termination that counteracts termination signals are essential processes of RNA synthesis (1). Transcription termination can occur via two mechanisms in bacteria: intrinsic and factor-assisted. Most intrinsic terminators contain an inverted and repeated sequence that can base pair to itself once transcribed to create a stable hairpin loop (7–20 bp long), rich in GC pairs and followed by a run of U residues (usually seven to nine bases long). Termination occurs in two steps: the pausing of the RNAP within the U tract, a position where the DNA:RNA hybrid is the weakest, followed by RNA release upon folding of the terminator hairpin (2). For many bacterial operons, the mechanism of anti-termination relies on sequence signals in the 5′-untranslated region (5′-UTR) found upstream of gene coding sequences. Once transcribed, these leader regions can fold into at least two mutually exclusive RNA structures: an intrinsic terminator and an anti-terminator. Switching between different conformations of this transcribed region (i.e. terminator versus anti-terminator folding) controls the fate of the elongation complex, and thus the expression of the downstream gene. This riboswitch is controlled by diverse regulators that include accessory proteins, small molecules, uncharged tRNAs and translating ribosomes (1).

The phosphoenol–pyruvate phosphotransferase system (PTS) regulation domains (PRDs)-containing anti-termination proteins belong to a class of regulatory proteins, which control the expression of genes involved in carbohydrate uptake and metabolism in bacteria. The representative member of this protein family is BglG from *Escherichia coli*, controlling the expression of a cryptic operon for β-glucoside utilization (3). Most members of this protein family are found in Gram-positive bacteria where they stimulate the transcription of various genes and operons in response to the presence of specific sugars. *Bacillus subtilis*, the model organism of Gram-positive bacteria, possesses four PRD-containing anti-termination proteins: LicT, the orthologue of *E. coli* BglG, that stimulates the expression of the *licS* gene and *bglPH* operon (4); SacY and SacT controlling *sacB* and *sacPA*, respectively, involved in sucrose utilization (5,6);

*To whom correspondence should be addressed. Tel: +33 467 41 79 06; Fax: +33 467 41 79 13; Email: margeat@cbs.cnrs.fr

© The Author(s) 2013. Published by Oxford University Press.
This is an Open Access article distributed under the terms of the Creative Commons Attribution License (http://creativecommons.org/licenses/by-nc/3.0/), which permits non-commercial reuse, distribution, and reproduction in any medium, provided the original work is properly cited. For commercial re-use, please contact journals.permissions@oup.com.

and GlcT controlling the *ptsGHI* operon encoding the glucose-specific PTS permease, the phospho-carrier protein HPr and the general PTS enzyme I (7). These transcriptional regulators, as all the anti-termination proteins of the BglG family, present the same modular organization. RNA binding is mediated by a N-terminal co-anti-terminator (CAT) domain, which can recognize specific RNA sequences on its own, thus promoting anti-termination (8). At the C-terminus of CAT domains are linked two homologous regulation domains, PRD1 and PRD2, which are the targets of multiple phosphorylation reactions by the PTS on conserved histidines (9–11). Depending on their phosphorylation state, the PRDs prevent or not CAT domain interaction with RNA. When activated, these transcriptional regulators bind as homodimers to a ribonucleotidic anti-terminator (RAT) sequence in the 5′-UTR region of their targeted mRNAs and stabilize its hairpin fold (Figure 1A and B) (3,12,13). This binding prevents the formation of an overlapping terminator hairpin, which otherwise provokes the premature arrest of transcription between the promoter and the gene coding sequences.

From a structural point of view, LicT is by far the best characterized member of the BglG family (14,15). The activation of LicT involves a massive conformational rearrangement of the relative orientation of the monomers, which in turn results in the partial unfolding of the CAT-PRD1 linker helix, allowing CAT domains to dimerize and interact efficiently with RNA (15,16). This activation is constitutive in the H207D/H269D double mutant (named LicT* herein), which mimics the phosphorylation of the corresponding histidines, as well as in isolated CAT domains (17). Crystallographic and NMR structural studies of the LicT-CAT domain, alone or in complex with its 29-nt RAT target showed that it folds as a β-stranded homodimer, and provided a rationale for how a symmetric dimer interacts with an apparently asymmetric RNA hairpin (8,18–20).

These anti-terminator RAT hairpins have been defined as 29-nt long sequences that share a common fold, where a variable apical loop and two asymmetrical internal loops interrupt a central stem (21) (Figure 1D). LicT-CAT domain interacts only with the bases from the internal loops and the central stem of the anti-terminator hairpin (Figure 1D, residues in *licS*-RAT highlighted in grey). Given the very high sequence similarities shared by the CAT domains on one hand and their cognate RAT hairpins on the other hand, it is very likely that the overall interaction mode observed for the LicT-CAT–RAT complex is conserved in orthologous and paralogous systems. However, significant differences in the sequence, structure and stability of the interacting partners are present and determine the relative affinity and specificity of the different CAT–RAT complexes. Several studies have shed some light on the sequence and structural features that underlie these specific interactions, and how cross-talk between these conserved systems is prevented or minimized (13,14,20,22,23). Two main differences can be noted in the natural *sacB*-RAT recognized by SacY compared with *licS*-RAT. First, a G–U wobble base pair might be present in the Loop 1 of *sacB*, which could result in its stabilization. In *licS*-RAT, this Guanine 26 is replaced with an adenine, which is expelled out of the helix axis in the presence of LicT, making specific contacts with the protein (20). Second, the basal stem of *licS*-RAT contains two additional Watson–Crick base-pairing bonds as compared with *sacB*-RAT (i.e. 2 GC + 2 AU base pairs instead of 2GC, respectively) leading to a 33-nt long hairpin instead of 29 nt, respectively. Although these additional base pairs are not located within the regions contacted by the protein (Figure 1D), they might confer to the hairpin a structure that influences the protein-binding affinity and the anti-termination activity. Interestingly, we observed (Supplementary Figure S1) that the RAT hairpins of the gene targets predicted to be recognized by LicT or its orthologues are of variable lengths (29, 31, 33 or 35 nt), while those predicted to be recognized by SacY and/or SacT orthologues are only 29- or 31-nt long (basal stem = 2GC + 1AU, 1 GC or 1 wobble GU). The predicted GlcT targets are generally shorter (29 nt) and the anti-terminator/terminator overlapping sequence is longer (9–15 nt) compared with that of the LicT or SacY/SacT gene targets (5–9 nt).

In this study, we sought to investigate how the length and the sequence, and thus the structure and stability of these anti-terminators hairpins influence the binding properties of the anti-termination proteins, and the competition by the terminator RNA sequence. We designed three anti-terminator hairpins (Figure 1C and D): $licS_{33}$, which contains the natural RAT sequence of the *B. subtilis licS* gene; $sacB_{33}$, which contains the natural 29 nt *sacB*-RAT sequence and a 4-bp basal stem identical to that of $licS_{33}$; and $sacB_{29}$, identical to $sacB_{33}$, but with a 2-bp basal stem. We first quantified the binding of LicT and SacY to these anti-terminator hairpins by fluorescence anisotropy. We then used single-molecule Förster Resonance Energy Transfer (smFRET) to monitor directly the opening and closing of these RNA structures and thus compare their stabilities, in the context of a competition by a terminator mimic and/or upon protein binding. We show that the length of the basal stem is the main determinant of the stability of these RNA hairpins. It thus governs the ability of the anti-termination proteins to bind and further stabilize them, and precludes the competitive folding of the terminator hairpins.

MATERIALS AND METHODS

Nucleic acids preparation

Atto647N-labelled RNA oligos were purchased from IBA Gmbh (Goettingen, Germany). DNA oligos were purchased from Eurogentec (Angers, France). Amino(dT) oligos were labelled using Cy3B succinimidyl ester, and purified using reverse phase HPLC. Hybridization was performed by heating the various complementary RNA/DNA strands at 90°C for 10 min in TE buffer, and slowly cooling down at room temperature.

Protein expression and purification

Wild-type (WT) and mutant full-length LicT (277 residues) were produced as N-terminal His-tag proteins

using a pQE30 vector (Qiagen). The SacY-CAT (56 residues) or LicT-CAT (57 residues) domains were purified as protein fusions with the N-terminal glutathione-S-transferase (GST) using the vector pGEX-2T (Amersham). Production in *E. coli* BL21(DE3) and the purification procedures by affinity chromatography and size exclusion chromatography have been described in details previously (24). Aliquots of the proteins were stored at −80°C in gel-filtration buffer containing 10 mM Tris pH 8, 0.2 mM EDTA, 2 mM DTT and 50 mM NaCl (WT LicT) or 300 mM NaCl (mutant LicT and all the GST–CAT fusions). Before use, aliquots were centrifuged and the protein concentration was determined by OD measurements at 280 nm using a NanoDrop spectrophotometer.

RAT sequences alignment

RAT sequences in complete bacterial genomes have been searched using the nucleotide blastn web server, hosted by the NCBI server (http://blast.ncbi.nlm.nih.gov) and the RAT sequences of *licS, sacB, sacX, sacP* or *ptsG* from *B. subtilis*. Each putative RAT sequence has been checked manually and only those for which the downstream regulated gene and the cognate anti-terminator protein could be unambiguously inferred have been retrieved. The identified target genes have been eventually renamed as their orthologues in *B. subtilis* or *E. coli*. Formation of the predicted downstream terminator hairpins have been checked using the RNAfold server (http://rna.tbi.univie.ac.at). No apparent RAT-overlapping terminator could be found in case of sacX encoding the negative SacY-regulator in the three *B. subtilis* sub-species we analysed, RNAfold detecting only an imperfect palindrome (Supplementary Figure S1, in grey) overlapping the RAT sequence over only 3 or 5 nt (underlined in black) and comprising a very small putative terminator (in red); nevertheless, previous studies have shown that sucrose-induction of the sacXY operon relies on this regulatory RAT element as well as downstream sequences possibly forming alternative mRNA secondary structures (3).

Bacterial strains

bsu168, *B. subtilis* Marburg 168; bsuSPZ, *B. subtilis* sub-species spizizenii TU-B-10; bsuJS, *B. subtilis* JS; bam, *Bacillus amyloliquefaciens* FZB42; ban, *Bacillus anthracis* H9401; bat, *Bacillus atrophaeus* 1942; bli, *Bacillus licheniformis* ATCC 14580; bme, *Bacillus megaterium* WSH-002; eco, *E. coli* K12; efa, *Enterococcus faecalis* OG1RF; ent, *Enterobacter cloacae* EcWSU1; geo, *Geobacillus thermoglucosidasius* C56-YS93; lac, *Lactococcus lactis* subsp. lactis KF147; pba, *Paenibacillus polymixa* Y412MC10; sca, *Staphylococcus carnosus* TM300; smj, *Streptococcus mutans* LJ23; ssu, *Streptococcus suis* D12.

Fluorescence anisotropy assays

Fluorescence anisotropy titrations were performed in Corning NBS 384-well plates by adding 30 µl of Atto647N-labelled RNA (0.4 nM) to 30 µl of serial dilutions of purified proteins. Fluorescence polarization was measured at 25°C using a Tecan Saphire II plate reader, with the excitation wavelength set to 630 nm and the emission measured at 680 nm. Buffer conditions were 10 mM Tris (pH 8), 1 mM EDTA, 1 mM DTT, 75 µg/ml bovine serum albumin and NaCl at various concentrations.

smFRET with alternating-laser excitation

smFRET with alternating laser excitation (25) measurements were performed on a home-made confocal microscope. Alternating-laser excitation (ALEX) was achieved with a polychromatic modulator (AA-Optics, France) using 532- and 641-nm laser light, with alternation period of 100 µs, and duty cycle of 50%. Before entering the objective (Zeiss Plan Apochromat ×100, NA 1.4), the beams were spatially filtered through a single-mode fibre. Emitted photons were collected through the objective, focused on a 100-µm pinhole and refocused onto silicon avalanche photodiode detectors (SPCM AQR-14, Perkin Elmer) that were connected to a counting board (PCI-6602, National Instruments, Austin, TX, USA). The fluorescence was separated into two streams using a 630DRLP dichroic mirror (Omega Optical) and filtered in front of each APD [ET-BP 585/65 (Chroma filters) and 650LP (Omega Optical)]. Photons detected at the donor or acceptor channels were assigned to either the donor or acceptor excitation based on arrival time, and generated emissions $f^{A_{em}}_{D_{exc}}$, $f^{D_{em}}_{D_{exc}}$, $f^{A_{em}}_{A_{exc}}$ and $f^{D_{em}}_{A_{exc}}$. Emissions were analysed to identify fluorescence bursts, allowing calculation of E_{PR} and S for each molecule and construction of 2D E_{PR}-S and 1D E_{PR} histograms (25). Apparent FRET efficiencies are reported as E_{PR} ratios, according to (26)

$$E_{PR} = \frac{F^{FRET}}{F^{FRET} + F^{D_{em}}_{D_{exc}}}$$

where, $F^{FRET} = F^{A_{em}}_{D_{exc}} - dF^{A_{em}}_{A_{exc}} - lF^{D_{em}}_{D_{exc}}$; d is the acceptor direct excitation coefficient, and l is the donor-leakage coefficient (26). All data analyses were performed using a home-made Labview routine (National Instruments, Austin, TX, USA). Resulting E_{PR} histograms represent only the molecules containing a donor and an acceptor (based on a selection on the S parameter), and are displayed and fitted using Origin (Northampton, MA, USA). Buffer conditions for all measurements were 10 mM Tris (pH 8), 150 mM NaCl, 1 mM EDTA and 1 mM DTT.

RESULTS

Binding experiments reveal the roles of the basal stem length and electrostatic interactions on the interaction of LicT and SacY with RNA

The energetics of binding to RAT hairpins of full length or CAT domains of LicT and SacY were determined by fluorescence anisotropy-binding experiments using RNA oligonucleotides labelled at their 5′-end with the Atto647N fluorescent dye (Figure 1). Figure 2 shows the binding isotherms obtained on $licS_{33}$, using full-length WT LicT (open circles) and the activated mutant LicT*

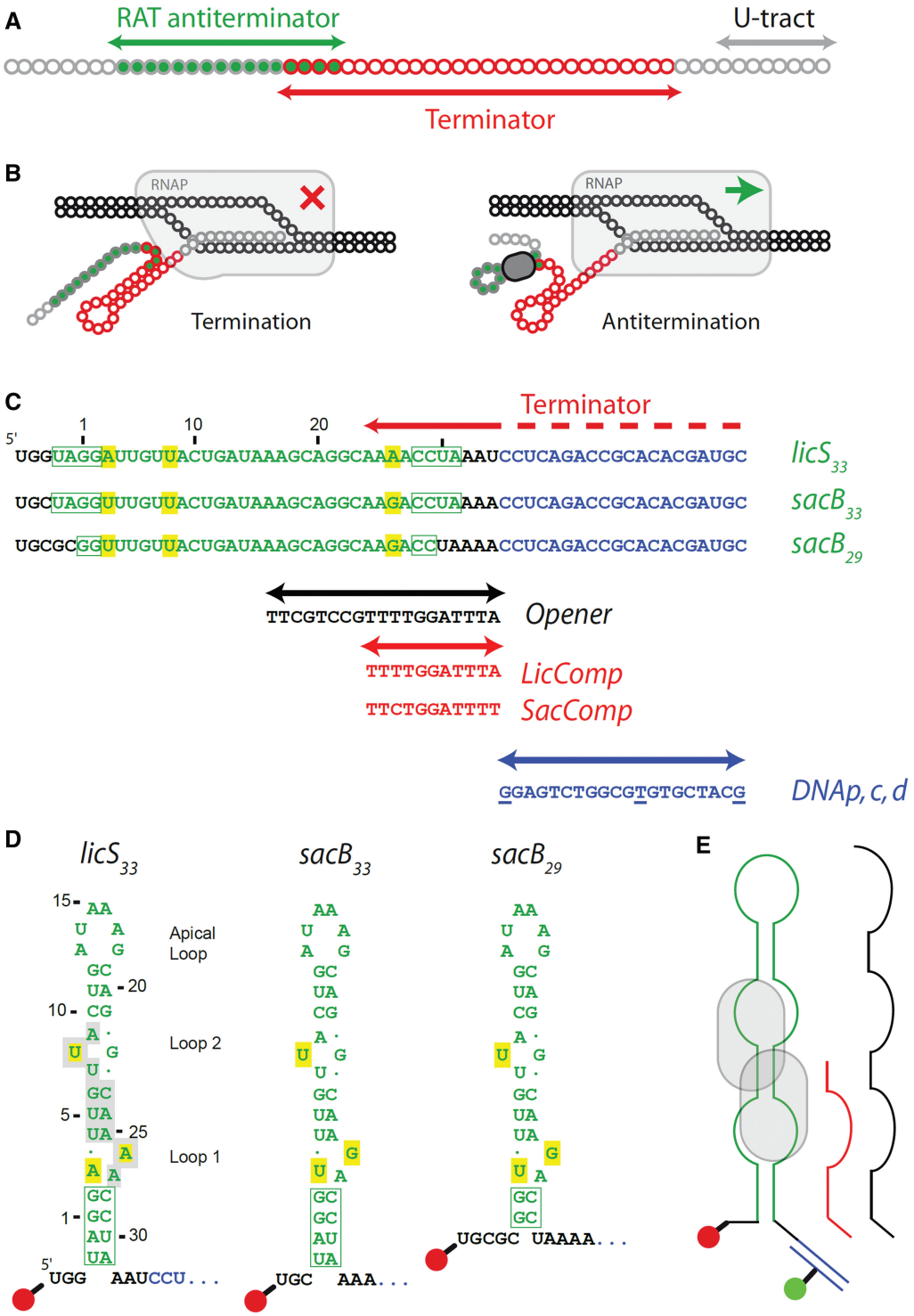

Figure 1. Principle of the anti-termination and nucleic acids constructs. (**A**) Schematic of the transcribed RNA of a typical anti-terminator/terminator system. The RAT anti-terminator hairpin (green filled dots) and the terminator hairpin (red dots) are partially overlapping, and thus competing for their complete closing. They are followed by a U-tract, that will be engaged in a weak DNA:RNA hybrid within the transcription elongation complex. (**B**) Schematic representation of the termination induced by the closing of the terminator hairpin (left) and the anti-termination promoted by the stabilization of the RAT hairpin, precluding the closing of the terminator hairpin (right). (**C**) *licS*$_{33}$, *sacB*$_{33}$ and *sacB*$_{29}$ RNA anti-terminator sequences. The green letters correspond to the RAT hairpins (33 or 29 nt). The blue letters correspond to the bases to be hybridized to the complementary DNA sequence for smFRET experiments (*DNAc*). The bases that are engaged into the basal stem are boxed, and the specificity determinants in RAT internal loops 1 and 2 as proposed by Aymerich and Steinmetz (12) are highlighted in yellow. The regions that will be hybridized by the *opener*, *comp* and *DNAc* oligos are represented by arrows and by their sequence. The *opener* oligo will induce a complete opening of the hairpin by hybridizing up to A16, while *comp* will mimic the hybridization caused by the terminator, up to A24, located in the stem between loops 1 and 2. The position of the cy3B donor label is underlined in the three different DNA oligonucleotides [DNAp: proximal (firstG); DNAc: central (T); DNAd: distal (last G)]. (**D**) Folded anti-terminators hairpins, showing the various loops, and the basal stem (boxed in green), whose size

(continued)

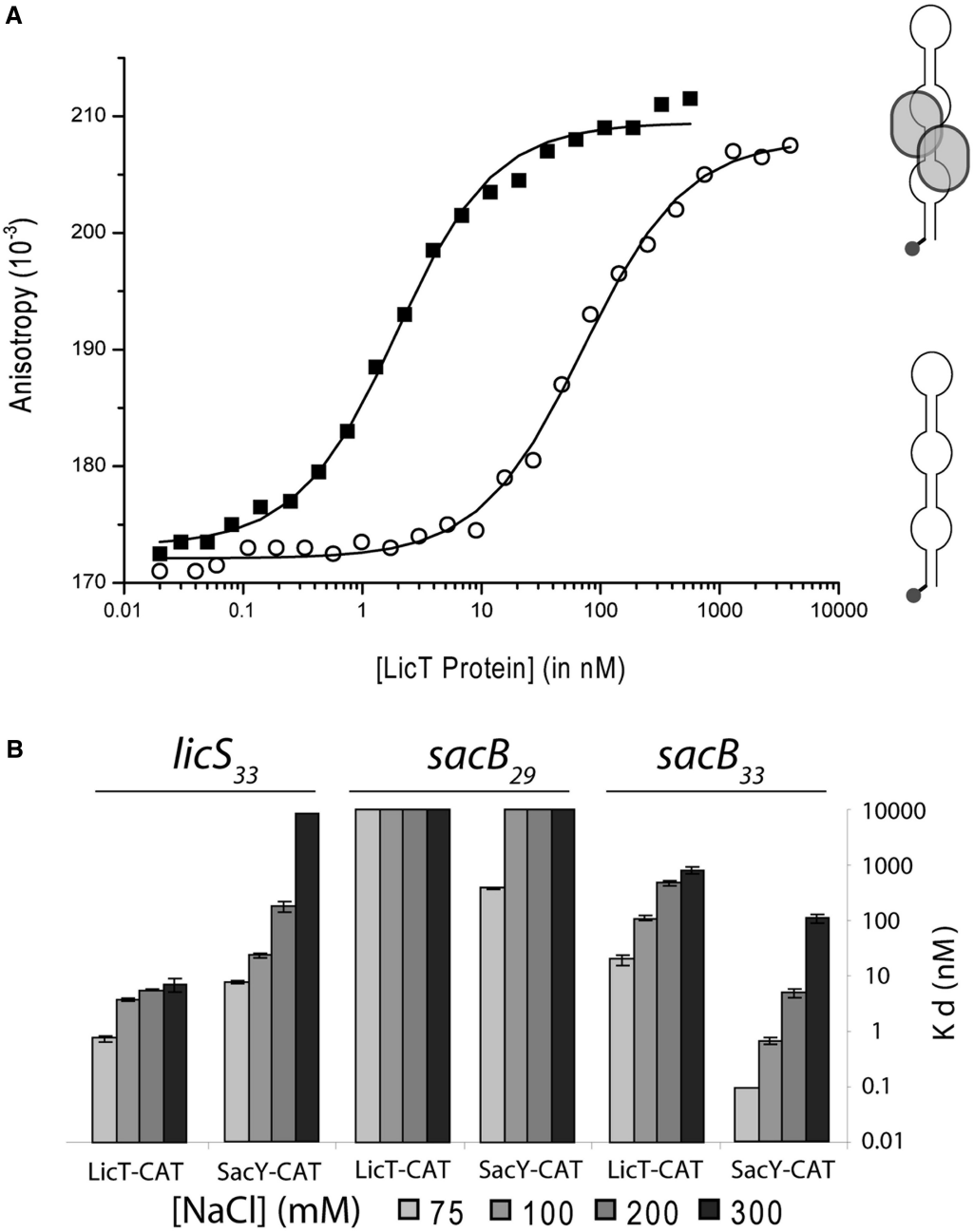

Figure 2. Fluorescence anisotropy titrations of anti-terminator hairpins by full-length LicT or LicT- and SacY-CAT domains. (**A**) Fluorescence anisotropy titrations of Atto647N-labelled *licS*$_{33}$ (0.2 nM) by full-length WT LicT (open circles) or its activated mutant LicT* (filled squares). Data were analysed and fitted with a 2:1 protein–RNA interaction model using the program BIOEQS. (**B**) Dissociation constants determined using fluorescence anisotropy titrations of Atto647N-labelled *licS*$_{33}$, *sacB*$_{33}$ and *sacB29* by the CAT domains from the anti-termination protein LicT and SacY. Various monovalent salt concentrations were used to explore the electrostatic contribution to the binding. The error bars correspond to the uncertainties at the 67% confidence limit in the determination of the binding energies (28). The K_d values <0.1 nM [that cannot be accurately determined since this correspond to stoichiometric titration conditions (38)] are displayed as 0.1 nM, without error bar. The K_d values > 10 μM (that cannot be accurately determined since this would require a high concentration of protein to cover the whole binding curve), are displayed as 10 μM, without error bar.

Figure 1. Continued
decreases from 4 to 2 bp for *sacB*$_{29}$ relative to *licS*$_{33}$ and *sacB*$_{33}$. On *licS*$_{33}$, the nucleotides shown to be interacting directly with the protein (20) are highlighted in grey, while the specificity determinants in RAT internal loops 1 and 2 as proposed by Aymerich and Steinmetz (12) are highlighted in yellow. The fluorescent label position (Atto647N) is represented by a red dot. (**E**) Schematic representation of the RNA anti-terminators hairpin (green). The complementary *DNAc* oligo used in smFRET experiments is represented in blue, together with the position of the donor fluorescent dye (Cy3B, green dot). The dimeric CAT domain of the anti-termination proteins is represented in grey. On the side, the regions that will be hybridized by the *opener* (black) and *comp* (red) oligos are represented as well.

($LicT_{H207D/H269D}$) (filled squares) (19). These isotherms were analysed using the BIOEQS software (27), using a 2:1 protein–RNA interaction model, and the recovered binding free energies are reported as dissociation constants (K_d) values ± the uncertainties at the 67% confidence limit in the determination of the binding energies (28). As expected, the LicT activating mutations leads to an increase in binding affinity (from 72 ± 6 to 1.8 ± 0.3 nM), consistent with the qualitative increase in binding affinity observed using gel-shift assays or surface plasmon resonance (19), and with the 40-fold increase in transcription anti-termination efficiency *in vivo* reported for this constitutive mutant relative to the WT (17). The K_d values measured here for the native and activated forms of full-length LicT are also in good agreement with the binding constants estimated previously for native and activated LicT CAT-PRD1 constructs in which the RNA-binding domain is fused to a WT or mutant PRD1 (15).

Having established the fluorescence anisotropy assay as a reliable method to investigate the binding of LicT to Atto647N-labelled $licS_{33}$, we performed a set of binding experiments, using $licS_{33}$, $sacB_{33}$ and $sacB_{29}$ as substrates, and the CAT domains from LicT or SacY as titrating proteins. For these experiments we used GST fusions of the isolated CAT domains, instead of full-length proteins, since full-length SacY is unstable *in vitro* (8). These GST–CAT fusions have previously been shown to behave as the CAT domains alone in RNA-binding assays *in vitro* (8,24). Our binding experiments were performed at various concentrations of monovalents salts (75, 100, 200 and 300 mM NaCl), and the recovered binding free energies are reported on Figure 2B and Supplementary Table S1, as dissociation constants (K_d) values.

These data reveal that LicT-CAT binds strongly and specifically to its cognate target ($licS_{33}$, K_d values <10 nM under all conditions). SacY-CAT can bind efficiently to $licS_{33}$ (K_d values of 25 ± 3 nM at 100 mM NaCl) but not to $sacB_{29}$, the 29-nt long hairpin corresponding to the natural *sacB*-RAT (K_d values >10 μM at 100 mM NaCl and above). Strikingly, with the $sacB_{33}$ construct that has two additional base pairs closing the hairpin as compared with $sacB_{29}$, a massive increase of the binding affinities (several orders of magnitude) is observed for both proteins. For example, at 200 mM NaCl, SacY-CAT binds to $sacB_{33}$ with the same affinity as LicT-CAT for $licS_{33}$ (5.5 ± 0.9 versus 6.1 ± 0.1 nM, respectively). The length of the basal stem closing the RAT hairpin is thus a key element of RNA recognition for both LicT and SacY. In addition, the specificity of SacY-CAT for its cognate *sacB*-RAT sequence is also improved by extending the *sacB*-RAT hairpin, the affinity being >40-fold higher for $sacB_{33}$ compared with $licS_{33}$. Conversely, the $sacB_{33}$ hairpin can be efficiently recognized by LicT-CAT, but with a 100 times lower affinity compared with $licS_{33}$ (600 ± 65 versus 6.1 ± 0.1 nM at 200 mM NaCl, respectively). This confirms that the first internal loop of the anti-terminator hairpin, containing the 2 nt that differ between *licS*-RAT and *sacB*-RAT (A3/U3 and A26/G26, see Figure 1 and Supplementary Figure S1) constitutes the major specificity determinant of CAT–RAT interaction (12,20).

These series of measurements also reveal the very strong effect of electrostatic interactions on RNA binding by SacY-CAT, but not by LicT-CAT. For example, the K_d of SacY-CAT for $sacB_{33}$ increases by a factor of 180 when the NaCl concentration increases from 100 to 300 mM, (<0.7 ± 0.1 to 127 ± 21 nM) while the K_d of LicT-RAT for the same target only increases 8-fold (134 ± 14 to 1050 ± 150 nM), and its K_d for $licS_{33}$ only doubles (4.1 ± 0.3 to 7.8 ± 2 nM). High ionic strength thus inhibits dramatically RNA binding in case of SacY-CAT but only marginally in case of LicT-CAT. At low salt concentration (≤100 mM), SacY-CAT binds with sub-nanomolar affinity to $sacB_{33}$, even more strongly and more specifically than LicT to its cognate RNA target. This effect might at least partly reflect the fact that SacY-CAT contains more basic residues than LicT-CAT (pI = 9.6 versus 6.1, respectively).

Anti-terminator hairpins alone are fully closed in solution

The massive effect of the extension of the basal stem on the binding affinity observed for $sacB_{33}$ versus $sacB_{29}$ prompted us to design an experiment aimed at monitoring the open/closed state of the RAT hairpin, in solution. The three oligoribonucleotides used in the fluorescence anisotropy titrations, labelled at their 5′-end with Atto647N and extended at their 3′-end with an artificial 20-base sequence, were hybridized to a Cy3B-labelled DNA oligonucleotide (Figure 1C–E). We checked using fluorescence anisotropy titrations that the hybridization of this DNA to the 3′extension of the RAT hairpins does not change the binding properties of LicT (not shown). FRET was then used as a reporter of the spatial proximity between Cy3B (donor) and Atto647N (acceptor). Thus, a closure/opening of the hairpin is expected to produce an increase/decrease in FRET efficiency, respectively. We used confocal optical microscopy with ALEX (25,29) to detect and to quantify fluorescence of single molecules in solution transiting a femtolitre-scale observation volume. For each such single molecule, we used the donor–acceptor stoichiometry parameter, S, to select the doubly labelled complexes, and calculated their apparent energy transfer efficiency, E_{PR} (25,29). In order to maximize these changes in FRET efficiencies upon opening of the hairpin, we tested three DNA oligonucleotides differing by the position of the donor dye: proximal (3′-end of the DNA), central (on Thymidine 9) and distal (5′-end of the DNA) (Figure 1C and Supplementary Figure S2). We selected the central position (called *DNAc*), that would give the highest amplitude in FRET efficiency changes (see Supplementary Figure S2 and details described later). Figure 3A (left) shows a typical histogram, showing the E_{PR} distribution obtained for hundreds of single molecules of ($licS_{33}$ + *DNAc*) (at 50 pM). A single population is observed, displaying a high FRET efficiency (population centred around $E_{PR} \sim 0.8$). This high-energy transfer value corresponds to a closed state of the hairpin. It has been observed as well under the same conditions for ($sacB_{33}$ + *DNAc*) and ($sacB_{29}$ + *DNAc*) (see details described later and Figure 5). This closed state appears rather stable as it is observed

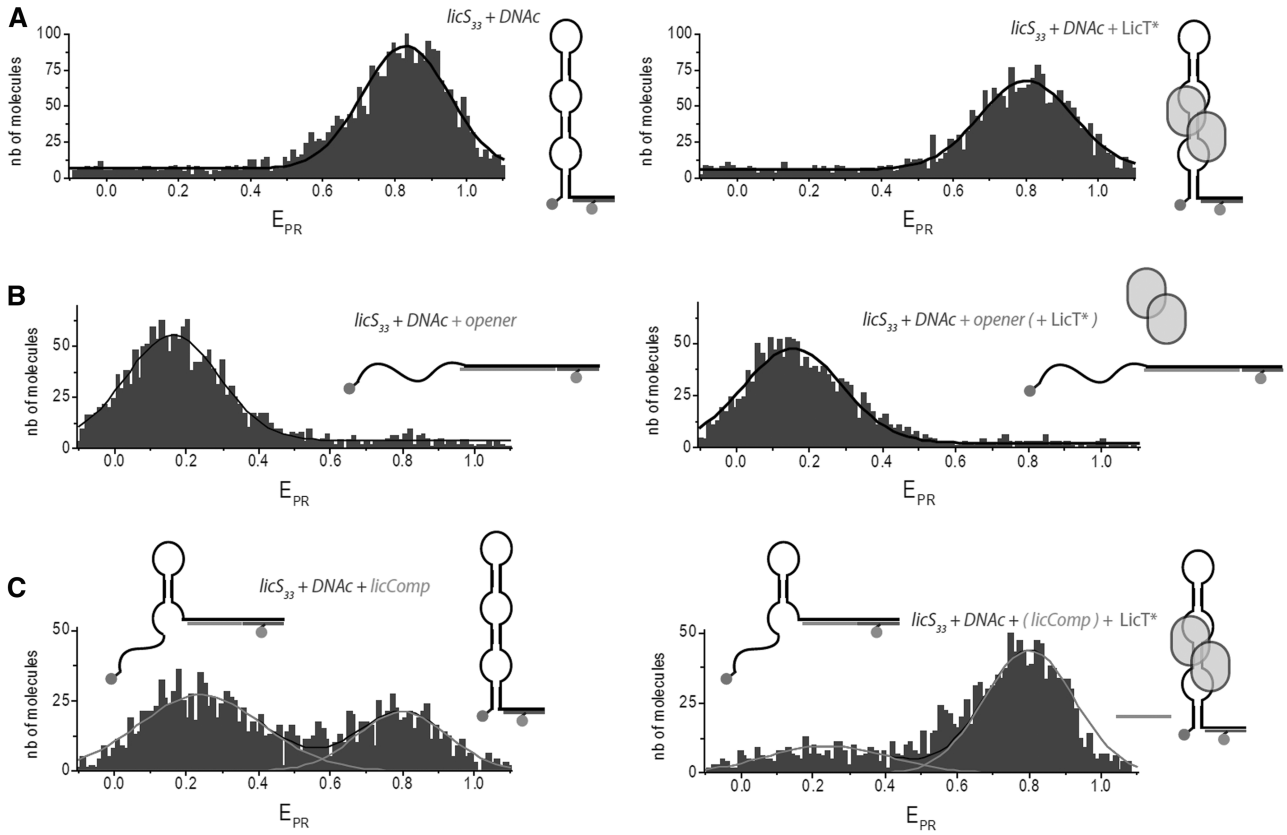

Figure 3. Detection of the anti-terminator hairpins opening and closing using smFRET. (**A**) Apparent energy transfer efficiency (E_{PR}) distribution obtained for hundreds of single diffusing molecules of the *licS33 + DNAc* doubly labelled RNA/DNA hybrids. A single distribution at high E_{PR} ($E_{PR} \sim 0.80$) is observed (left), consistent with a closed RNA hairpin structure. Upon addition of 100 nM LicT*, no change in the distribution is observed, indicating that LicT binding does not dramatically changes the hairpin structure. (**B**) Addition of the *opener* oligonuleotide at 5 μM to *licS33 + DNAc* induces the complete opening of the hairpin ($E_{PR} \sim 0.16$). Upon addition of 100 nM LicT*, no change in the distribution is observed, indicating that LicT is not able to bind to the RNA when the hairpin structure is completed disrupted. (**C**) Upon addition of 5 μM of the terminator mimic *licComp* to *licS33 + DNAc*, two populations are observed a fully closed ($E_{PR} \sim 0.80$) and an almost totally open state ($E_{PR} \sim 0.24$). Upon addition of 100 nM LicT*, the equilibrium is pushed toward the closed form of the hairpin, due to the stabilization of this state by the binding of the protein.

under a wide range of monovalent salt (NaCl) concentrations (from 100 to 400 mM), that have been shown to influence the stability of RNA hairpins (30,31) (Supplementary Figure S3). Similarly, addition of the divalent cation Mg^{2+} ($\leq$20 mM) does not change the position and the shape of the E_{PR} distribution, suggesting that Mg^{2+} does not promote any global conformational change in the hairpin structure (data not shown).

When 100 nM of the constitutively active LicT* (i.e. a saturating concentration) is added to (*licS33 + DNAc*) (50 pM), no change is observed in the E_{PR} distribution (Figure 3A, compare left and right), indicating that protein binding does not induce any additional folding of the RNA hairpin. Altogether, these data indicate that under our experimental conditions (20°C), the anti-terminator hairpins are stably and fully folded in solution. Thus, these hairpins already possess the folded structure that will be recognized by the anti-termination protein.

LicT* does not bind to a fully disrupted hairpin

We then wanted to promote a full opening of the *licS33* hairpin, in order to verify our ability to detect this conformational change using smFRET, and to test the binding of LicT to such a disrupted structure. We used a DNA oligonucleotide (*opener*, Figure 1C), which hybridizes with *licS33*, between the binding position of *DNAc* up to A16 in the apical loop of the RAT hairpin (Figure 1C–E). For the (*licS33 + DNAc*) (50 pM) + *opener* (5 μM) construct, a single population, centred around $E_{PR} \sim 0.16$, is observed (Figure 3B, left), demonstrating the opening of the *licS* RAT structure, and thus our ability to monitor the opening/closing transition with our method. When 100 nM of the constitutively active LicT* is added, no change is observed in the E_{PR} distribution (Figure 3B, compare left and right). This indicates that the protein, even in its activated form, is unable to bind to this completely disrupted RNA structure to induce its folding.

A terminator mimic induces the partial opening of the anti-terminator hairpin, which is reversed by protein binding

Next, we tested a set of oligonucleotides aimed at mimicking the terminator hairpins and designed to compete with the anti-terminator hairpins (*comp* oligos,

Figure 1C). Indeed, when a terminator hairpin is fully transcribed, and folds into a stem-loop structure, it precludes the complete closing of the partially overlapping anti-terminator hairpin (because of the competition mechanism for the same sequence). The *comp* oligos have the same sequence as the 3′-end of the terminator hairpin. They will thus bind to the anti-terminator hairpin, between *DNAc* and A24, and are expected to nucleate the opening of these hairpin structures (Figure 1C–E). While *licComp* will bind to $licS_{33}$, *sacComp* will target $sacB_{33}$ and $sacB_{29}$ (Figure 1C–E). Adding 5 μM of *licComp* to ($licS_{33}$ + *DNAc*) (50 pM) (Figure 3C, left) results in a bimodal distribution: ~70% of the molecules are in an open state ($E_{PR} \sim 0.24$), whereas 30% are in the closed state ($E_{PR} \sim 0.80$), which probably reflects the fractions of molecules where *licComp* is bound or not bound, respectively. The value of E_{PR} for the open state is slightly, but significantly higher than the one obtained for the fully open state induced by *opener* (0.24 versus 0.16), indicating that in the context of *licComp* binding, most of the $licS_{33}$ hairpins retain some residual, partially folded structure, that could correspond for example to the stem that closes the apical loop (see cartoon on Figure 3C, left, for illustration). When 100 nM of the constitutively active LicT* is added to ($licS_{33}$ + *DNAc*) (50 pM) + *licComp* (5 μM) (Figure 3C, right) the open/close equilibrium is pushed toward the closed form. This shows the ability of LicT* to bind to the $licS_{33}$ hairpin, as expected, and to stabilize the closed form. According to the classical model of anti-termination, this stabilizing effect precludes the terminator hairpin to fully hybridize and close itself, and thus precludes the premature arrest of transcription.

Competition assays reveal the stability of the anti-terminator hairpins

The proportion of $licS_{33}$ hairpin in the open versus closed state depends on the concentration of *licComp* in a dose dependent manner as shown on Figure 4. By determining the areas recovered from a double Gaussian fitting of the smFRET data, it is possible to determine directly the percentage of closed versus open hairpins. We performed these measurements for the three RNA hairpins with increasing concentration of their cognate competitor DNA [see Figure 5A, where data for $sacB_{29}$ (triangles), $sacB_{33}$ (open circles) and $licS_{33}$ (squares) are presented]. Although these constructs appear totally closed when alone in solution, they respond quantitatively differently to their respective terminator mimic oligonucleotides. The concentration of competitor necessary to promote 50% of $sacB_{29}$ opening is ~1 nM, whereas 300–1000 nM of competitor are necessary for $sacB_{33}$ or $licS_{33}$ opening. This high sensitivity of $sacB_{29}$ to the terminator competition underlines the stabilizing effect of the 4-bp basal stem of $sacB_{33}$ relative to the 2-bp basal stem of $sacB_{29}$. We note that this different effect cannot be accounted for by different binding energies of the competitor for $sacB_{33}$ versus $sacB_{29}$, since this competitor (*sacComp*) and the target sequence are the same. Performing the same competition assays in the presence of 10 μM LicT (Figure 5B) or 10 μM LicT* (Figure 5C) yields qualitatively similar results. The differences stand in the fact that it is necessary to add ~10 times more *Comp* in the presence of LicT, and 100 times more *Comp* in the presence of LicT*, to obtain a competing effect similar to the one observed in the absence of protein. This observation simply reflects the stabilizing effect of the protein on the closed form of the anti-terminator hairpins. We note that 20% of $sacB_{33}$ appears to remain in a closed state, even at maximal *licComp* concentration. This might be due to the fact that a fraction of $sacB_{33}$ might fold into a stable, alternative hairpin structure, which lacks the Loop 1 (Supplementary Figure S4). Thus, *licComp* binding and opening activity might be strongly reduced on this minor alternative RNA structure.

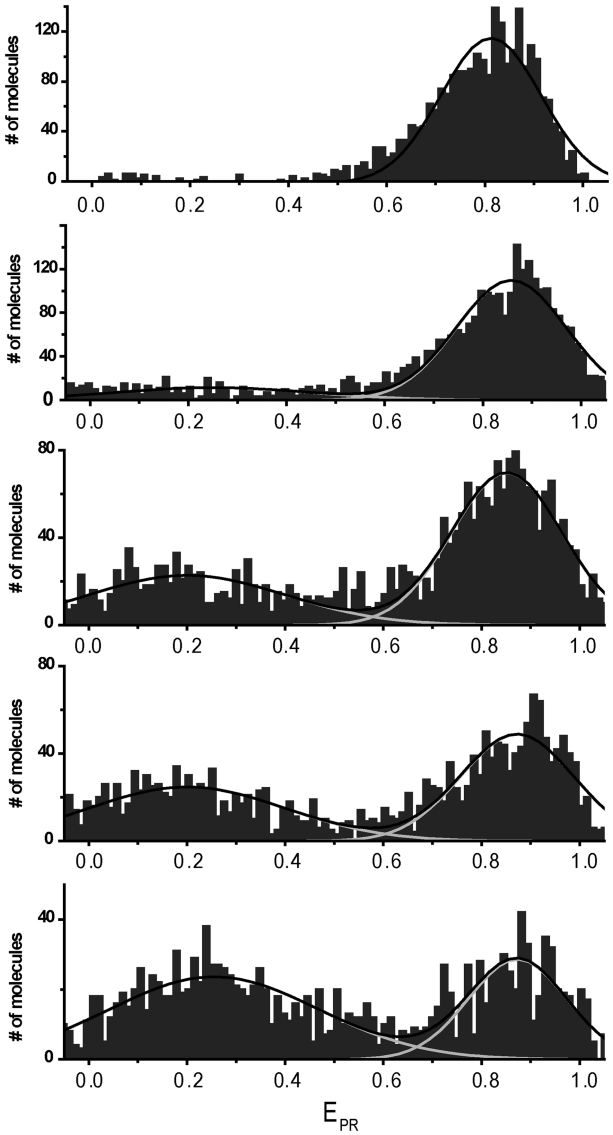

Figure 4. Titration of $licS_{33}$ + *DNAc* by increasing concentrations of the terminator mimic *licComp*. smFRET was used to monitor the opening of the $licS_{33}$ anti-terminator hairpin upon addition of increasing concentration of the *licComp* DNA (from top to bottom 0, 50, 500, 1000 and 2500 nM). The proportion of open $licS_{33}$ hairpins increases as a function of [*licComp*], demonstrating its dose-dependent competing effect.

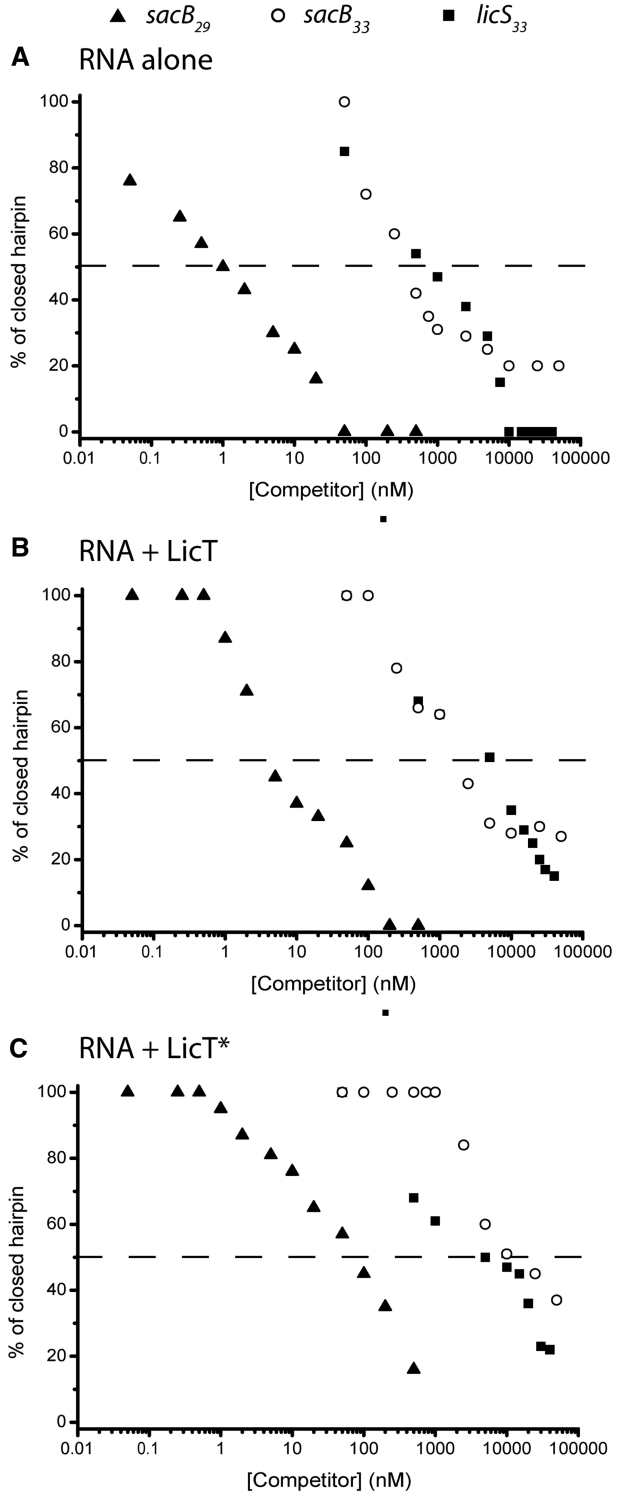

Figure 5. Opening of the anti-terminator hairpins with increasing terminator mimics concentration. Percentage of closed hairpins, determined using the areas recovered from a double Gaussian fitting of the smFRET data, as a function of competitor DNA (*comp*) concentration, and in the absence (**A**) or the presence of 10 μM native LicT (**B**) or 10 μM activated LicT* (**C**). Data are presented for $sacB_{29}$ (triangles), $sacB_{33}$ (open circles) and $licS_{33}$ (squares). The concentration of competitor DNA required for opening the RAT structure is about a 100-fold higher in the case of the intrinsically stabilized RAT hairpins ($sacB_{33}$ and $licS_{33}$) or in the presence of the activated anti-termination protein LicT*.

DISCUSSION

The molecular mechanism of terminator hairpin-induced dissociation of the transcription elongation complex, leading to transcription termination, remains a subject of debate (1,32–35). Precluding the formation of this terminator hairpin leads to anti-termination. We investigated in the present study several aspects of the competition between terminator versus anti-terminator hairpins folding. We generated a set of labelled nucleic-acid constructs based on *licS* and *sacB* anti-terminator sequences, and on competing terminator motifs. Using smFRET, we were able for the first time to monitor directly the structural dynamics of these anti-terminator hairpins, and thus investigate the determinants of the balance between the two competing structures, that determines the fate of the transcription complex. The canonical target for the PRD-containing anti-termination proteins was originally defined based on the 29-nt long consensus sequence targeted by the first identified members of the BglG family (3,12,21). In subsequent studies, the use of either 29-nt hairpins (12,13,23), or of longer hairpins artificially stabilized was generalized (24,22). Thus the effect of the flanking sequences that determine the total length of the RAT hairpin has been overlooked in the past. Here, our results reveal that the size and stability of the basal stem of the anti-terminator hairpins play a predominant role on their stability, and thus on their structure, the anti-termination proteins binding, and the terminator competition.

We first show that all the anti-terminator RAT sequences studied spontaneously fold into a closed structure under our experimental conditions (at 20°C), and that the anti-termination protein bind to these pre-formed anti-terminator hairpins without inducing additional folding, as observed in the LicT-CAT–RAT complex (20). These results are in apparent contradiction with earlier studies on the paralogous GlcT/*ptsG*-RAT system for which DNAseI footprinting experiments have indicated that the 'RAT exists in the single stranded form in the absence of GlcT and adopts the double-stranded conformation upon GlcT addition' (36). It cannot be excluded that, unlike *sacB*-RAT and *licS*-RAT, *pstG*-RAT cannot form a stable hairpin in the absence of the anti-termination protein. This explanation is however unlikely since our smFRET experiments show that within the timescales of our measurements for each molecule (typically 1 ms), all the RAT targets are mainly in a closed conformation when alone in solution, including the most unstable hairpin $sacB_{29}$ whose basal stem has the same length as that of *ptsG*-RAT. More likely, the apparent discrepancy between smFRET and DNAseI foot-printing results is due to different observation timescales. Even for the most stable RNA structures observed by smFRET, faster dynamics (in the microsecond timescales) are expected, allowing the opening of the hairpins for a small fraction of time. This can be sufficient for irreversible hydrolysis by DNAseI, leading to the observation of a foot-printing pattern, especially since these experiments were performed at 37°C, where a higher probability of hairpin opening is expected. Addition of the anti-termination protein

stabilizes the folded RNA, i.e. reduces its structural dynamics and thereby protects it against DNAseI attack. Previous NMR studies on a 31-nt *licS*-derived RAT hairpin are in good agreement with this explanation. Although the protein-free RNA structure could not be solved in solution due to high intrinsic dynamics, it presented secondary and tertiary structural elements identical to those observed for the stabilized RNA hairpin of the LicT-CAT–RAT complex [(20), Y. Yang and M. Kochoyan (personal communication)].

Another important finding of the present work is that the length, and thus the stability and the structure of the basal stem are major determinants of the affinity of binding of LicT and SacY, more than the sequence of the 29-nt hairpin itself. Indeed, both LicT-CAT and SacY-CAT have a better affinity for $sacB_{33}$ than for $sacB_{29}$ (Figure 2B). Since these proteins do not make any molecular contact to the basal stem (20), this fact underlines the crucial role of this basal stem on the hairpin stability and its folding into a conformation efficiently recognized by the proteins. Although the two *sacB*-derived hairpins appear globally folded in solution at the millisecond timescale, faster opening/closing processes might occur in $sacB_{29}$, leading to a structure that is less prone to be bound by the anti-termination proteins. In fact, the width of the E_{PR} histograms for the closed and open forms, for all the constructs studied, is wider than expected for a static structure with a fixed distance. This suggests that dynamic processes in the microsecond to millisecond timescales are taking place. We are currently investigating these fast dynamics processes using time-resolved experiments coupled to correlation analysis (37). Using this approach, it would also be interesting to determine whether the additional GU wobble base pair found in the natural *sacB* sequence is sufficient to further lock the basal stem, leading to SacY binding with higher affinity.

Our results also show that the CAT–RAT interactions specificity is also influenced by the length of the anti-terminator hairpin. Indeed, although SacY-CAT has the highest affinity for $sacB_{33}$, it has a better affinity for $licS_{33}$ than for $sacB_{29}$ derived from the natural *sacB*-RAT sequence (Figure 2B). Thus, the recognition of the RAT hairpins is less influenced by the specific protein/RNA contacts found in the 29-nt RAT sequence, in particular in internal loops 1 and 2 (Figure 1C), than by the stability of the basal stem. This is in good agreement with previous studies that have already pointed out that RNA structure rather than sequence are major specificity determinants (36). Interestingly, on the $sacB_{33}$ artificially stabilized construct we used here, SacY-CAT binds with a very high affinity, and a very good specificity (Figure 2B, compare SacY-CAT/$sacB_{33}$ with LicT-CAT/$licS_{33}$ and SacY-CAT/$licS_{33}$), as compared with what has been observed in the past using shorter constructs (24,23). Interpretation of some earlier results on the relative affinity and specificity of the different CAT–RAT complexes should thus be re-examined in the light of the present finding revealing the influence of the nucleotide sequence flanking the canonical 29-nt RAT hairpin. We also observed a strong effect of the ionic strength on SacY-CAT specific binding, as compared with LicT-CAT. This suggests that the way SacY and LicT discriminates between RAT sequences relies on different types of protein–nucleic acid interactions, as suggested by earlier studies aiming at the identification of amino acid residues involved in differential RNA binding (19,23).

Finally, we found that the balance between the anti-terminator and terminator folding, which is the basis of the regulatory mechanism by anti-termination, is also strongly influenced by the size of the basal stem of the RAT hairpin. Using a terminator mimic that competes with nucleotides of the hairpin basal stem, we found that it is necessary to use ~500 times more competitor to induce the opening of the RAT structure in case of $sacB_{33}$ than of $sacB_{29}$. This strong effect is also observed in the presence of the activated mutant LicT*, that binds to all the RATs with higher affinity, and thus stabilizes more their closed structures. Extending the *sacB*-RAT hairpin by two Watson–Crick base-pairs thus greatly enhanced the stability of the anti-terminator hairpin and the strength of the anti-termination complex. This result confirms and extends the observation that replacing an AU pair with the GC pair in an anti-terminator hairpin derived from *ptsG* induces an increase in transcription anti-termination *in vivo*, in a β-galactosidase assay (13). Moreover, our smFRET results on $sacB_{33}$ suggest the presence of more stable alternative RNA structures, that cannot be unfolded by the terminator-mimic (Figure 5; Supplementary Figure S4). *In vivo*, this could severely jeopardize the formation of the terminator even when transcription of the downstream metabolic gene is not required, leading to constitutive expression or important read-through. A fine adjustment of the interactions involving residues in the basal stem of the anti-terminator/terminator hairpins is thus crucial for the regulation process. In contrast, the intrinsic stability of the terminator would play a minor role, as judged from the very variable length of the terminator sequences identified upstream of genes and operons predicted to be regulated by anti-termination proteins of the BglG family (Supplementary Figure S1). However, it is interesting to note that the length of the anti-terminator hairpin basal stem and of its overlap with the terminator appears as a well conserved feature within each class of anti-termination proteins. Further studies will be necessary to determine whether these different sizes of RAT hairpins are driving the balance between termination and anti-termination *in vivo*.

SUPPLEMENTARY DATA

Supplementary Data are available at NAR Online: Supplementary Table 1, Supplementary Figures 1–4 and Supplementary Reference [39].

ACKNOWLEDGEMENTS

The authors thank the IBiSA Structural Biology platform of the Centre de Biochimie Structurale for its help in

protein production and purification. They thank Catherine Royer and Soraya Bouhours Ait-Bara (CBS) for critical reading of this manuscript.

FUNDING

The Agence Nationale de la Recherche (ANR) Programme Blanc, (TERMINATOR); Ministère de la Recherche (ACI BCMS); GIS 'IBiSA: Infrastructures en Biologie Sante et Agronomie'. Funding for open access charge: CNRS.

Conflict of interest statement. None declared.

REFERENCES

1. Santangelo,T.J. and Artsimovitch,I. (2011) Termination and antitermination:RNA polymerase runs a stop sign. *Nat. Rev. Microbiol.*, **9**, 319–329.
2. Gusarov,I. and Nudler,E. (1999) The mechanism of intrinsic transcription termination. *Mol. Cell.*, **3**, 495–504.
3. Mahadevan,S. and Wright,A. (1987) A bacterial gene involved in transcription antitermination: regulation at a rho-independent terminator in the bgl operon of *E. coli*. *Cell*, **50**, 485–494.
4. Schnetz,K., Stülke,J., Gertz,S., Krüger,S., Krieg,M., Hecker,M. and Rak,B. (1996) LicT, a *Bacillus subtilis* transcriptional antiterminator protein of the BglG family. *J. Bacteriol.*, **178**, 1971–1979.
5. Arnaud,M., Vary,P., Zagorec,M., Klier,A., Debarbouille,M., Postma,P. and Rapoport,G. (1992) Regulation of the sacPA operon of *Bacillus subtilis*: identification of phosphotransferase system components involved in SacT activity. *J. Bacteriol.*, **174**, 3161–3170.
6. Debarbouille,M., Arnaud,M., Fouet,A., Klier,A. and Rapoport,G. (1990) The sacT gene regulating the sacPA operon in *Bacillus subtilis* shares strong homology with transcriptional antiterminators. *J. Bacteriol.*, **172**, 3966–3973.
7. Stülke,J., Martin-Verstraete,I., Zagorec,M., Rose,M., Klier,A. and Rapoport,G. (2003) Induction of the *Bacillus subtilis* ptsGHI operon by glucose is controlled by a novel antiterminator, GlcT. *Mol. Microbiol.*, **25**, 65–78.
8. Manival,X., Yang,Y., Strub,M.P., Kochoyan,M., Steinmetz,M. and Aymerich,S. (1997) From genetic to structural characterization of a new class of RNA-binding domain within the SacY/BglG family of antiterminator proteins. *EMBO J.*, **16**, 5019–29.
9. Deutscher,J., Francke,C. and Postma,P.W. (2006) How phosphotransferase system-related protein phosphorylation regulates carbohydrate metabolism in bacteria. *Microbiol. Mol. Biol. Rev.*, **70**, 939–1031.
10. Postma,P.W., Lengeler,J.W. and Jacobson,G.R. (1993) Phosphoenolpyruvate:carbohydrate phosphotransferase systems of bacteria. *Microbiol. Rev.*, **57**, 543–594.
11. Stulke,J., Arnaud,M., Rapoport,G. and Martin-Verstraete,I. (1998) PRD–a protein domain involved in PTS-dependent induction and carbon catabolite repression of catabolic operons in bacteria. *Mol. Microbiol.*, **28**, 865–874.
12. Aymerich,S. and Steinmetz,M. (1992) Specificity determinants and structural features in the RNA target of the bacterial antiterminator proteins of the BglG/SacY family. *Proc. Natl Acad. Sci. USA*, **89**, 10410–10414.
13. Schilling,O., Herzberg,C., Hertrich,T., Vörsmann,H., Jessen,D., Hübner,S., Titgemeyer,F., Stülke,J., Vo,H., Hu,S. *et al.* (2006) Keeping signals straight in transcription regulation: specificity determinants for the interaction of a family of conserved bacterial RNA-protein couples. *Nucleic Acids Res.*, **34**, 6102–6115.
14. van Tilbeurgh,H. and Declerck,N. (2001) Structural insights into the regulation of bacterial signalling proteins containing PRDs. *Curr. Opin. Struct. Biol.*, **11**, 685–693.
15. Demene,H., Ducat,T., De Guillen,K., Birck,C., Aymerich,S., Kochoyan,M. and Declerck,N. (2008) Structural mechanism of signal transduction between the RNA-binding domain and the phosphotransferase system regulation domain of the LicT antiterminator. *J. Biol. Chem.*, **283**, 30838–30849.
16. Graille,M., Zhou,C.Z., Receveur-Brechot,V., Collinet,B., Declerck,N. and van Tilbeurgh,H. (2005) Activation of the LicT transcriptional antiterminator involves a domain swing/lock mechanism provoking massive structural changes. *J. Biol. Chem.*, **280**, 14780–14789.
17. van Tilbeurgh,H., Le Coq,D., Declerck,N., Tilbeurgh,H.V. and Coq,D.L. (2001) Crystal structure of an activated form of the PTS regulation domain from the LicT transcriptional antiterminator. *EMBO J.*, **20**, 3789–3799.
18. van Tilbeurgh,H., Manival,X., Aymerich,S., Lhoste,J.M., Dumas,C. and Kochoyan,M. (1997) Crystal structure of a new RNA-binding domain from the antiterminator protein SacY of *Bacillus subtilis*. *EMBO J.*, **16**, 5030–5036.
19. Declerck,N., Dutartre,H., Receveur,V., Dubois,V., Royer,C., Aymerich,S. and van Tilbeurgh,H. (2001) Dimer stabilization upon activation of the transcriptional antiterminator LicT. *J. Mol. Biol.*, **314**, 671–681.
20. Yang,Y., Declerck,N., Manival,X., Aymerich,S. and Kochoyan,M. (2002) Solution structure of the LicT-RNA antitermination complex: CAT clamping RAT. *EMBO J.*, **21**, 1987–1997.
21. Houman,F., Diaz-Torres,M.R. and Wright,A. (1990) Transcriptional antitermination in the bgl operon of *E. coli* is modulated by a specific RNA binding protein. *Cell*, **62**, 1153–1163.
22. Declerck,N., Minh,N.L., Yang,Y., Bloch,V., Kochoyan,M. and Aymerich,S. (2002) RNA recognition by transcriptional antiterminators of the BglG/SacY family: mapping of SacY RNA binding site. *J. Mol. Biol.*, **319**, 1035–1048.
23. Hübner,S., Declerck,N., Diethmaier,C., Le Coq,D., Aymerich,S., Stülke,J., Hu,S., Coq,D.L., Hubner,S. and Stulke,J. (2011) Prevention of cross-talk in conserved regulatory systems: identification of specificity determinants in RNA-binding anti-termination proteins of the BglG family. *Nucleic Acids Res.*, **39**, 4360–4372.
24. Declerck,N., Vincent,F., Hoh,F., Aymerich,S. and van Tilbeurgh,H. (1999) RNA recognition by transcriptional antiterminators of the BglG/SacY family: functional and structural comparison of the CAT domain from SacY and LicT. *J. Mol. Biol.*, **294**, 389–402.
25. Kapanidis,A., Lee,N.-K., Laurence,T., Doose,S., Margeat,E. and Weiss,S. (2004) Fluorescence-aided molecule sorting. Analysis of structure and interactions by alternating laser excitation of single molecules. *Proc. Natl Acad. Sci. USA*, **101**, 8936–8941.
26. Lee,N.K., Kapanidis,A.N., Wang,Y., Michalet,X., Mukhopadhyay,J., Ebright,R.H. and Weiss,S. (2005) Accurate FRET measurements within single diffusing biomolecules using alternating-laser excitation. *Biophys. J.*, **88**, 2939–2943.
27. Royer,C.A. (1993) Improvements in the numerical analysis of thermodynamic data from biomolecular complexes. *Anal. Biochem.*, **210**, 91–97.
28. Boyer,M., Poujol,N., Margeat,E. and Royer,C.A. (2000) Quantitative characterization of the interaction between purified human estrogen receptor alpha and DNA using fluorescence anisotropy. *Nucleic Acids Res.*, **28**, 2494–2502.
29. Kapanidis,A.N., Laurence,T.A., Lee,N.K., Margeat,E., Kong,X. and Weiss,S. (2005) Alternating-laser excitation of single molecules. *Acc. Chem. Res.*, **37**, 523–533.
30. Lambert,D., Leipply,D., Shiman,R. and Draper,D.E. (2009) The influence of monovalent cation size on the stability of RNA tertiary structures. *J. Mol. Biol.*, **390**, 791–804.
31. Bizarro,C.V., Alemany,A. and Ritort,F. (2012) Non-specific binding of Na+ and Mg2+ to RNA determined by force spectroscopy methods. *Nucleic Acids Res.*, 1–14.
32. Larson,M.H., Landick,R. and Block,S.M. (2011) Single-molecule studies of RNA polymerase: one singular sensation, every little step it takes. *Mol. Cell*, **41**, 249–262.

33. Larson,M.H., Greenleaf,W.J., Landick,R. and Block,S.M. (2008) Applied force reveals mechanistic and energetic details of transcription termination. *Cell*, **132**, 971–982.
34. Epshtein,V., Cardinale,C.J., Ruckenstein,A.E., Borukhov,S. and Nudler,E. (2007) An allosteric path to transcription termination. *Mol. Cell*, **28**, 991–1001.
35. Santangelo,T.J. and Roberts,J.W. (2004) Forward translocation is the natural pathway of RNA release at an intrinsic terminator. *Mol. Cell*, **14**, 117–126.
36. Schilling,O., Langbein,I., Müller,M., Schmalisch,M.H. and Stülke,J. (2004) A protein-dependent riboswitch controlling ptsGHI operon expression in *Bacillus subtilis*: RNA structure rather than sequence provides interaction specificity. *Nucleic Acids Res.*, **32**, 2853–2864.
37. Felekyan,S., Kalinin,S., Sanabria,H., Valeri,A. and Seidel,C.a.M. (2012) Filtered FCS: species auto- and cross-correlation functions highlight binding and dynamics in biomolecules. *ChemPhysChem*, **13**, 1036–1053.
38. Weber,G. (1992) *Protein Interactions*. Chapman and Hall, London.
39. Zuker,M. (2003) Mfold web server for nucleic acid folding and hybridization prediction. *Nucleic Acids Res.*, **31**, 3406–3415.